Quaternary Science Reviews 280 (2022) 107415

Contents lists available at ScienceDirect

Quaternary Science Reviews

journal homepage: www.elsevier.com/locate/quascirev

Glacial isostatic adjustment in the Red Sea: Impact of 3-D Earth structure

Barra A. Peak [a, 1, *], Konstantin Latychev [a], Mark J. Hoggard [a, b], Jerry X. Mitrovica [a]

[a] Department of Earth and Planetary Sciences, Harvard University, 20 Oxford St, Cambridge, MA, 02318, USA
[b] Research School of Earth Sciences, Australia National University, 142 Mills Rd, Acton ACt 0200, Australia

ARTICLE INFO

Article history:
Received 5 September 2021
Received in revised form
29 January 2022
Accepted 2 February 2022
Available online 17 February 2022

Handling Editor: C. O'Cofaigh

Keywords:
Sea level changes
Last glacial maximum
Numeric modeling
Mantle viscosity
Holocene

ABSTRACT

Sea-level history in the Red Sea region has commonly been interpreted as an accurate proxy for global mean sea level (GMSL), which can be used to constrain global ice volumes and inform a diverse range of regional paleoclimate studies. Previous modeling work has demonstrated, however, that glacial isostatic adjustment (GIA) processes may introduce significant departures from GMSL in this region. The GIA signal is a complex combination of deformational, gravitational, and rotational effects arising from shifting ice and water surface loads and consists of long-wavelength effects superimposed by a short-wavelength signal associated with “continental levering” – a response to local meltwater loading. In this study, we revisit the effects of GIA in the Red Sea region using Earth models characterized by 3-D variations in mantle viscoelastic structure and lithospheric thickness, focusing on the period from Last Glacial Maximum (LGM) to present day. We find that the presence of the Red Sea Rift and low-viscosity upper mantle acts to amplify sea-level rise associated with continental levering, yielding a more pronounced rise for sites toward the center of the Red Sea during deglaciation in comparison to GMSL. In contrast, coastal sites experience a net GIA-induced sea-level fall that acts in opposition to the GMSL rise. Furthermore, while the maximum departure from GMSL occurs close to LGM for northern sites, the GIA signal can peak as late as 14 ka for southern sites. Simulations based on 3-D Earth models tend to show a smaller departure from GMSL than 1-D predictions for most coastal sites, including at the Strait of Bab el-Mandeb at the mouth of the Red Sea, and typically peak at ~10 m. The opposite is true for sites close to the rift: at these locations the difference between the 1-D and 3-D simulations can reach ~20 m. We therefore conclude that any mapping from local sea level to GMSL is both location and time dependent and cannot be captured by a simple linear scaling.

1. Introduction

Estimates of global mean sea level (GMSL) variations across the ice age cycles of the Late Pleistocene represent a key constraint on models of glacial isostatic adjustment (GIA) effects on sea level and the geophysical, climatological, and archaeological applications of such modeling. GIA effects lead to a departure of local sea level from GMSL. The GIA signal is driven by changing ice and water masses on the surface of the Earth and reflects perturbations in the Earth's shape, gravity field and rotational state. GMSL estimates are commonly derived from analyses of preserved coral reef terraces at low-latitude sites (e.g. Lambeck and Chappell, 2001; Peltier and Fairbanks, 2006) or from oxygen isotope records from deep sea sedimentary cores (e.g. Lisiecki and Raymo, 2005), but both approaches have drawbacks. In the first, GIA processes imprint a strong geographic variability in sea level and corrections for this heterogeneity face significant uncertainties in ice history and Earth structure (e.g. Austermann et al., 2013; Dendy et al., 2017; Lambeck et al., 2014). Meanwhile the second approach is complicated by the dual sensitivity of oxygen isotope records to ice volume and ocean temperature. This non-uniqueness has been addressed by recent efforts to simultaneously analyze variations in multiple isotopic ratios, for example Mg/Ca (Shakun et al., 2016).

Abbreviations: GMSL, global mean sea level; GIA, glacial isostatic adjustment; LGM, last glacial maximum.

* Corresponding author.
E-mail addresses: barra.peak@colorado.edu (B.A. Peak), latychev@fas.harvard.edu (K. Latychev), mark.hoggard@anu.edu.au (M.J. Hoggard), jxm@eps.harvard.edu (J.X. Mitrovica).
[1] Present address: Department of Geological Sciences, University of Colorado, Boulder, 2200 Colorado Ave, CO 80309, USA.

https://doi.org/10.1016/j.quascirev.2022.107415

The Hanish Sill is located in the Strait of Bab el-Mandeb (connecting the Red Sea to the Gulf of Aden; Fig. 1) and, at a minimum of 137 m below sea level, marks the shallowest point within the Strait at modern times (Werner and Lange, 1975). Siddall et al. (2003, 2004), building on an earlier study by Rohling et al. (1998), combined oxygen isotope records from sediment cores within the Red Sea with hydraulic modeling of water flux across the sill to estimate depth as a function of time since 470 ka. They interpreted this sea-level record at the Strait as an accurate proxy for “global sea level.” The unprecedented, centennial scale temporal resolution of their record over most of the last glacial phase (70–25 ka) has led to a diverse range of applications wherein this record is used as a proxy for GMSL, including studies of global climate change, hominin archeology, ecosystem biology, and many others (e.g. Rohling et al., 2008; Grant et al., 2012; Goñi, 2020; Antonioli et al., 2021; Peresani et al., 2021). However, the assumption that any difference between local sea-level changes at the Strait and GMSL is negligible ignores contributions from GIA. Lambeck et al. (2011) subsequently modeled GIA-induced sea-level changes across the region over several glacial cycles, with a particular focus on the Last Interglacial (ca. 120 ka) and the Late Holocene (8–0 ka). They found that during these two periods, local relative sea level could differ by approximately 5 m and 2 m, respectively, across sites spanning the region.

The Lambeck et al. (2011) analysis was based on one-dimensional (1-D), depth-varying models of the Earth's viscoelastic structure, an assumption that is common to the vast majority of GIA modeling studies. The Red Sea region is, however, characterized by significant three-dimensional (3-D) variations in Earth structure, reflective of its complex tectonic and mantle dynamic setting (e.g., Chu and Gordon, 1998; Eagles et al., 2002; Mohriak and Leroy, 2012; Hansen et al., 2008; Hammond et al., 2013; Wilson et al., 2014). A mid-oceanic spreading center, with active rifting since at least Miocene times (e.g. Purser and Bosence, 1998), runs through the center of the region and separates the African (Nubian) Plate to the southwest from the Arabian Plate to the northeast, which is characterised by progressively thicker, cratonic lithosphere (Hoggard et al., 2020, Figs. 1 and 2A). The spreading center is terminated to the north by the Sinai microplate and to the south by the Danakil microplate, which acts as the western boundary of the Strait of Bab el-Mandeb. Seismic tomography indicates that the spreading ridge is underlain by a large-scale slow shear-wave velocity anomaly – inferred to be hot, buoyant mantle – that originates in the deep mantle below southern Africa (Ritsema et al., 2011). The anomaly reaches the upper mantle beneath the East African Rift, where it impinges on the lithosphere beneath the Afar Triple Junction and has been connected both to this rifting (Ritsema et al., 1999) and up-on-the-southwest tilting of the Arabian Plate (Daradich et al., 2003; Wilson et al., 2014).

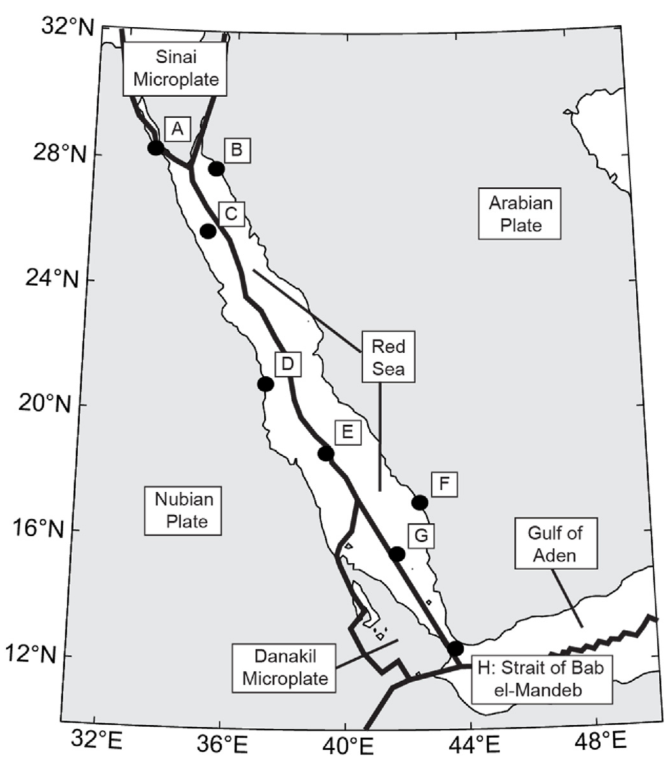

Fig. 1. Tectonic setting for the Red Sea region and selected sea-level sites used in this study. Plate boundaries are marked with thick black lines and individual plates and microplates are labelled.

In this study we predict sea-level changes in the Red Sea region using a high-resolution GIA model (Austermann et al., 2013; Latychev et al., 2005) that incorporates realistic, 3-D variations in mantle viscoelastic structure that are constrained by a range of geophysical and geological data. The focus of our study is the period from Last Glacial Maximum (LGM) to present day. Our goals are twofold. First, we aim to investigate the sensitivity of GIA-based sea-level reconstructions to lateral variations in mantle and lithospheric structure in this rift tectonic setting. Second, we want to quantify the error introduced by the assumption that local sea-level records in the Red Sea, particularly at the Strait of Bab el-Mandeb, are representative of GMSL. The relevance of the results extends beyond issues of ice age climate. Indeed, the Red Sea region is one of the oldest sites of human civilization and sea-level changes likely played an important role in human settlement and migration (White et al., 2003; Bailey, 2009; Lambeck et al., 2011; Bailey et al., 2017).

2. Numerical modeling

Our results are based on the finite-volume Maxwell viscoelastic model of GIA processes developed by Latychev et al. (2005) with a variable grid resolution reaching ~4 km at the surface within the Red Sea basin. The simulations solve for gravitationally self-consistent sea-level variations using a theory that extends the treatment of Farrell and Clark (1976) to accurately account for shoreline migration, changes in the perimeter of grounded, marine-based ice sheets, and the impact of perturbations in Earth rotation on sea level (Kendall et al., 2005; Mitrovica et al., 2005; Mitrovica and Milne, 2003). The modeling requires two main inputs: the space-time geometry of ice cover (the “ice history model”) and the 3-D elastic lithosphere thickness and mantle viscosity field (the “Earth model”). We describe each of these in turn.

Our ice-history model is based on ICE-5G (Peltier, 2004) with several modifications. The first involves a reduction in ice volumes equivalent to a GMSL change of 2 m at 8 ka, tapering to 0 m at 4 ka. Goldberg et al. (2016) demonstrated that this modification is necessary to fit the relative sea-level record at Samothrace, an eastern Mediterranean site close to the Red Sea region. Second, we adjust the pre-LGM ice history in the manner described by Pico et al. (2016), such that GMSL at 45 ka is set to −40 m relative to

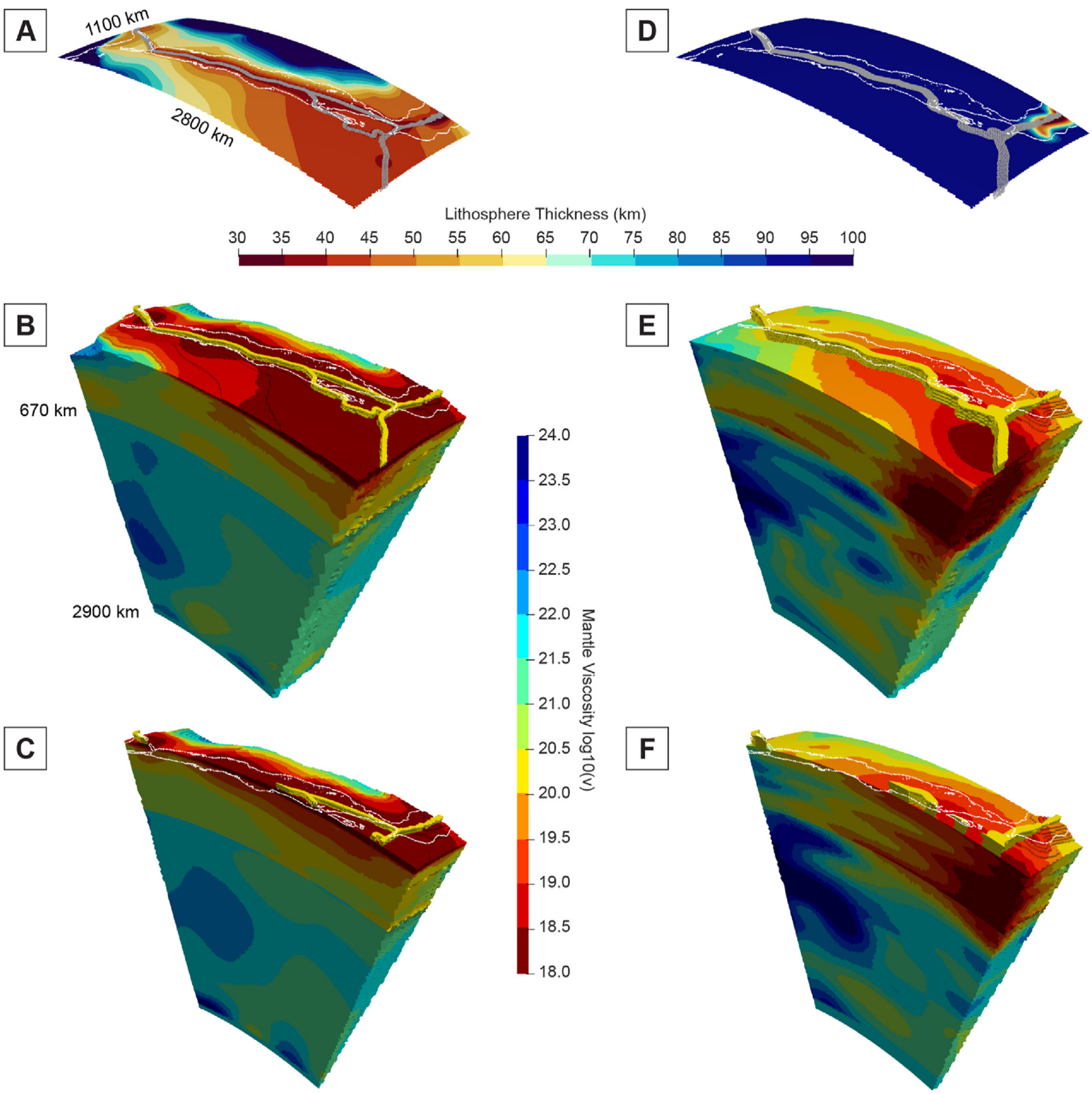

Fig. 2. 3-D Earth models for the Red Sea region. A) Lithospheric thickness for model M3D$_A$ overlain with plate boundaries (gray lines) with width set equal to the underlying lithospheric thickness up to a maximum 72.5 km. B) 3-D Cutaway showing mantle viscosity on a logarithmic scale. The upper surface corresponds with the base of the lithosphere and plate boundaries are demarcated by yellow lines. C) Same, but with the long-axis cut directly beneath the Red Sea spreading center. D-F) Same as A-C but for model M3D$_B$. Plate boundary width determined as in model M3D$_A$. Texture in the 3-D rendering corresponds to the tetrahedral grids used in modeling, which have an approximate 4 km spatial resolution at the surface increasing to 12 km at depth. (For interpretation of the references to colour in this figure legend, the reader is referred to the Web version of this article.)

present day. We initiate our simulations at ~50 ka; in this case, the Maxwell time of the adopted Earth models is sufficiently short to ensure that the LGM to present-day predictions of relative sea level are insensitive to earlier ice mass variations. Adoption of a different ice model for the period leading into the LGM and in the subsequent deglaciation would have an impact on the GIA predictions, in particular the difference between 1D and 3D simulations. Nevertheless, the location of the Red Sea, in the far field of ice cover, will mean that this impact will be relatively small compared to the effects at a site in the near field of ice cover (e.g. Hay et al., 2017; Powell et al., 2021).

We adopted four Earth models in our simulations: two 1-D Earth models and two 3-D Earth models. All models have 1-D density and elastic structure prescribed from the seismic model PREM (Dziewonski and Anderson, 1981). The two 1-D Earth models are characterized by upper (<670 km depth) and lower mantle viscosities of 5×10^{20} Pa s and 5×10^{21} Pa s respectively. They are distinguished on the basis of the thickness of the elastic lithosphere: 49 km and 96 km. These models are referred to as REF49 and REF96.

The first 3-D model – M3D$_A$ – is adopted from Austermann et al. (2021) (Fig. 2A–C). The model is constructed in three steps. First, a global seismic velocity anomaly model is generated by combining models SL2013sv in the upper mantle (Schaeffer and Lebedev, 2013) with SEMUCB-WM1 in the lower mantle (French and Romanowicz, 2015). Next, the shear-wave velocity anomalies are converted to temperature and then viscosity using anelastic parameters taken from mineral physics experiments and calibrated using measurements of seismic attenuation and thermal structure of the oceanic lithosphere (Richards et al., 2020). The model is constrained to have a spherically averaged viscosity structure identical to the above 1-D models: 5×10^{20} Pa s and 5×10^{21} Pa s in the upper and lower mantle, respectively. Finally, the model uses the depth of the 1175 °C isotherm to establish global elastic lithospheric thickness variations (Hoggard et al., 2020), but we patch in a higher resolution lithosphere model based on the seismic inferences of Hansen et al. (2008) for areas in the Red Sea and Arabian Shield (Fig. 2A). Plate boundaries for the region are taken from Bird (2003) with the addition of a segment defining the eastern boundary of the Danakil microplate (Fig. 1). These boundaries are modeled as weak zones with effective viscosities 1/3 that of the underlying reference upper mantle viscosity and with effective width equal to the local lithospheric thickness. A hard maximum width bound is set to 72.5 km (Fig. 2A). We note that simulations based on model $M3D_A$ treat the Danakil Depression, an area of low topography located on the Danakil Microplate and Nubian-Danakil plate boundary, as being disconnected from the Red Sea and subareal. We also performed calculations in which the depression was allowed to fill with water and found that the resulting impact on sea-level predictions was negligible.

The second 3-D model ($M3D_B$; Fig. 2D–F) is adopted from earlier work (Hay et al., 2017) with regional mantle viscosity modifications as described in Goldberg et al. (2016). This model was adopted as an intermediate complexity test case relative to model $M3D_A$ and the two 1-D models. $M3D_B$ is based on global seismic shear wave model S40RTS (Ritsema et al., 2011) patched together with regional model ECOS-TU-42 (Fichtner et al., 2013) and converted to a viscosity field as discussed in Austermann et al. (2013). Lithospheric thickness variations (Fig. 2D) are adopted from Conrad and Lithgow-Bertelloni (2006). In earlier work, there were refinements to this model for the Antarctic region (Hay et al., 2017), but those changes are irrelevant to the predictions described here since they impact only the near-field region of ice cover. Plate boundaries are once again taken from Bird (2003), however the boundary on the eastern side of the Danakil Microplate is in this case omitted to simplify the model. Plate boundary effective viscosity and width are derived as in Model $M3D_A$ using the lithospheric thickness model of Conrad and Lithgow-Bertelloni (2006) (Fig. 2B). As in model $M3D_A$, the spherically averaged viscosity structure of $M3D_B$ is equivalent to that of the 1-D viscosity profiles.

As described above, the two 3-D models differ significantly in thickness of the lithosphere but are similar in upper mantle viscosities values ranging from 1×10^{18} Pa s to 1×10^{24} Pa s. A notable difference between the viscosity structures of the two models is that the low viscosity region below the Afar Triple Junction extends much deeper into the upper mantle in model $M3D_B$ relative to $M3D_A$ (Fig. 2E and F), reflecting a significant plume stem below the Afar hotspot (Ritsema et al., 1999, 2011). This stem is less prominent in $M3D_A$, in keeping with Hammond et al. (2013).

3. Results and discussion

We evaluate results for all four models at eight sites within the Red Sea region covering the central trough and coastal areas and spanning the entire north-to-south extent of the sea (Fig. 1). The three trough sites lie adjacent to or on the plate boundary and have been selected to correspond with the locations of drill cores used to construct the sea-level curve of Siddall et al. (2003, 2004). The coastal sites, including the Strait of Bab el-Mandeb, were selected to provide coverage along the full length of the sea, including both its eastern and western coastlines.

Fig. 3 shows sea level relative to present (relative sea level; RSL) predictions at each site. RSL predictions are a combination of GMSL and net GIA effects, as described in full in Milne and Mitrovica (2008) and Mitrovica and Milne (2002). The net GIA signal is a combination of three effects. One, loss of gravitational attraction between ice sheets and the ocean due to melting of the ice sheets beginning at LGM initiates a migration of water away from the near field due to loss of gravitational attraction, contributing a sea-level rise from LGM to present-day at the Red Sea in the far field. Two, ocean syphoning (i.e., movement of water away from far-field locations driven largely by subsidence of a crustal bulge at the periphery of regions of former ice cover) contributes a lowering of sea level from LGM to present day in the Red Sea. Third, continental levering (i.e., subsidence of oceanic crust and uplift of the adjacent continent along coastlines due to meltwater loading of the lithosphere) tends to raise sea level at sites within the Red Sea from LGM to present day. The predictions in Fig. 3, whether based on 1-D or 3-D Earth models, tend to show a lower magnitude of total sea-level rise from LGM to present day in comparison to GMSL (with the exception of 3-D predictions at site E and the $M3D_A$ prediction at sites C and G). This pattern indicates that the primary GIA signal across the region is a net sea-level fall compared to GMSL, driven by ocean syphoning. At the Strait of Bab el-Mandeb, the RSL results for all models (Fig. 3H) are consistent with the previous work of Lambeck et al. (2011) and Siddall et al. (2004), who found that the Red Sea was not isolated from the global oceans at LGM since modern water depths at this site are >137 m and modeled RSL reaches at most 122 m below present levels.

Both the gravitational and syphoning signals are long wavelength, imparting a muted gradient across the Red Sea, whilst continental levering imprints a strong regional signal at shorter wavelengths, which provides most of the variation in GIA signal observed. Fig. 4 shows maps of the difference between predicted local sea level and GMSL at LGM (22 ka), 18 ka and 14 ka for all four model simulations. The further one moves seaward from the coast, the more negative the difference between GIA and GMSL and the greater the sea-level rise due to continental levering. Indeed, close to the plate boundary at the center of the Red Sea (sites C, E and G), the sign of the GIA signal is negative or close to zero for models $M3D_A$ and $M3D_B$, with the exception of site G, where the signal is positive for $M3D_B$ (Fig. 5). This indicates that, from LGM to present day, the levering signal is significant enough within this region to lead to a net GIA-induced sea-level rise greater than that associated with GMSL alone. It is also clear in Fig. 4 that the levering signal for the two 3-D simulations is significantly greater than predicted in the two 1-D simulations. The reason for this effect is that the thin lithosphere at, and proximal to, the plate boundary in combination with relatively low upper mantle viscosities (Fig. 2), leads to a greater subsidence of the crust in response to ocean loading than in the two 1-D models. Thus, there is a greater local compensation of the far-field syphoning signal, yielding a net sea-level rise.

Fig. 5 shows the difference between RSL predictions and GMSL for each of the four Earth models across the past 30 ka at our eight comparison sites. With the exception of sites C, E and G, the remaining sites are coastal and the total GIA signal at LGM and

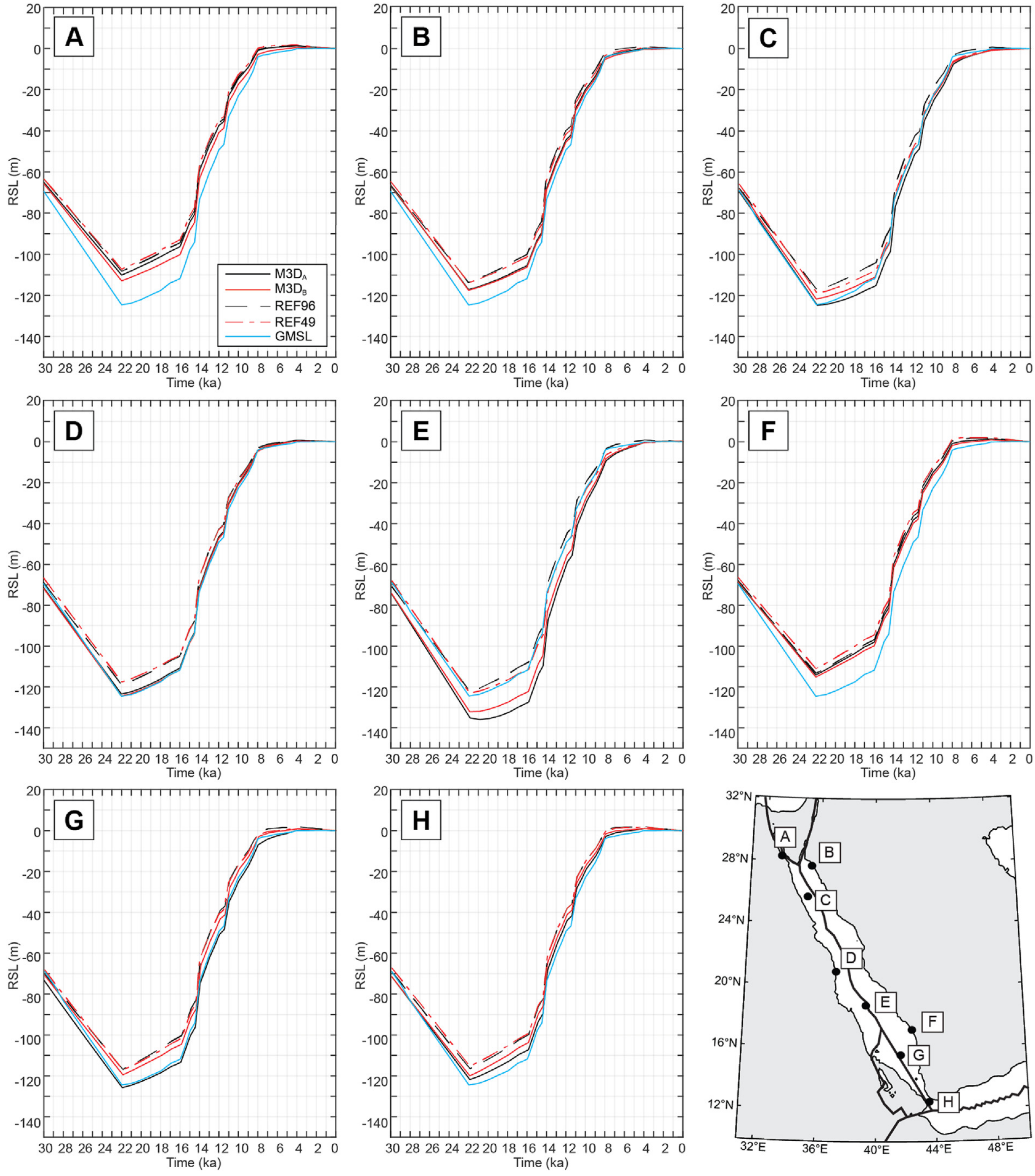

Fig. 3. Relative sea-level (RSL) predictions from 30 ka to present at eight sites (see inset map) for all four Earth models used in this study. The global mean sea level (GMSL) curve for the adopted ice history is also shown (light blue). The legend is consistent for all panels. (For interpretation of the references to colour in this figure legend, the reader is referred to the Web version of this article.)

extending to the present-day is mostly positive (yellow to red zones in Fig. 4); i.e., GIA acts to reduce total sea-level rise from LGM to present day. Site E, in contrast, is located close to the plate boundary and the levering signal is great enough to result in a mostly negative difference between GIA and GMSL (a net GIA-induced sea-level rise) that is particularly pronounced in the 3-D simulations. Site G is also located close to the plate boundary, but in an area in which the Red Sea narrows towards its mouth at the Strait of Bab el-Mandeb. This factor limits the amplitude of the levering signal and only simulation M3D$_A$ predicts a net GIA-induced sea-level rise. Site C, which is located between the coast and plate boundary, also exhibits a limited levering signal, with only M3D$_A$ predicting a net GIA-induced sea-level rise.

The time series in Fig. 5 indicate that the greatest departure

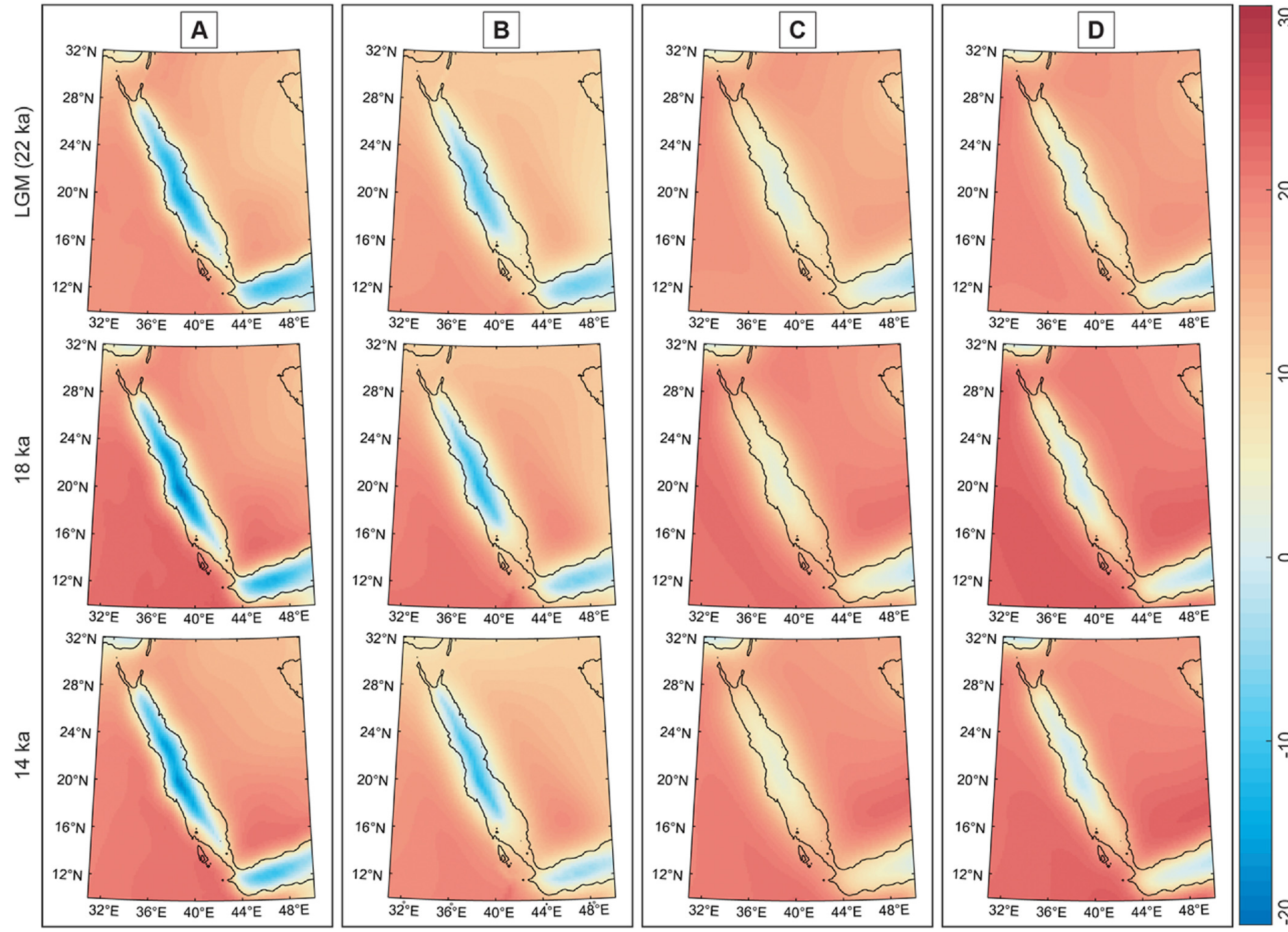

Fig. 4. Difference between RSL and GMSL predictions at LGM (22 ka), 18 ka and 14 ka for **A)** Model M3D$_A$, **B)** Model M3D$_B$, **C)** Model REF96, and **D)** Model REF49.

from GMSL (i.e., the largest GIA-induced signal) occurs close to LGM at most northern sites (sites A-D) but thousands of years later at southern sites in the Red Sea (sites E-H). This delay and signal migration can also be seen, though to a smaller extent, by comparing the three rows of Fig. 4, particularly for model M3D$_A$.

As noted in Section 1, the relative sea-level curve reconstructed by Siddall et al. (2003) is commonly interpreted as a proxy for GMSL. The results shown in Figs. 4 and 5 indicate that the discrepancy between local sea level and GMSL is dependent on both time and location, hence any mapping between the two is not a simple linear scaling. These results also indicate that 3-D Earth structure has a significant impact on the predicted GIA signal and any local sea level departures from GMSL. The difference between the 1-D and 3-D predictions varies by location and ranges from a few meters up to ~20 m. It is interesting to note that the introduction of lateral variations in Earth structure tends to bring local sea level closer to GMSL at the Strait of Bab el-Mandeb (site H), where sea level was inferred to be representative of GMSL in previous studies. Nevertheless, at 14 ka, a maximum departure from GMSL of 6 m and 9 m occurs for simulations M3D$_A$ and M3D$_B$, respectively. 9 m is approximately equivalent to the volume of Eurasian ice cover at 14 ka in the ICE-5G ice model (Peltier, 2004). Thus, assuming local sea level from the Strait to be equivalent to GMSL would result in a major misestimation of global ice volume history.

Lambeck et al. (2011) noted discrepancies between geologic observations and their reconstructions of local RSL changes based on 1-D GIA models and speculated that they might reflect additional tectonic activity in the region. The calculations performed here suggest that these discrepancies may arise, at least in part, from the neglect of lateral variations in Earth structure inherent to 1-D modeling. Use of 3-D variations in mantle viscoelastic structure in sea-level models within the region may therefore also inform reconstructions of regional tectonic history. If these discrepancies can be reconciled by the inclusion of 3-D Earth structure in future studies, then appeal to tectonic activity may no longer be necessary.

Sea-level reconstructions for the Holocene and earlier also have implications for human migration and settlement in the Red Sea area. The Red Sea was part of prominent human migration routes and provided food and means of transportation for early civilizations (e.g. Bailey, 2009; Bailey et al., 2017; Lambeck et al., 2011). The paleo-bathymetry of the Red Sea would have had a large impact on where humans settled and crossed the water body. The GIA models presented in this study generally predict Holocene sea levels closer

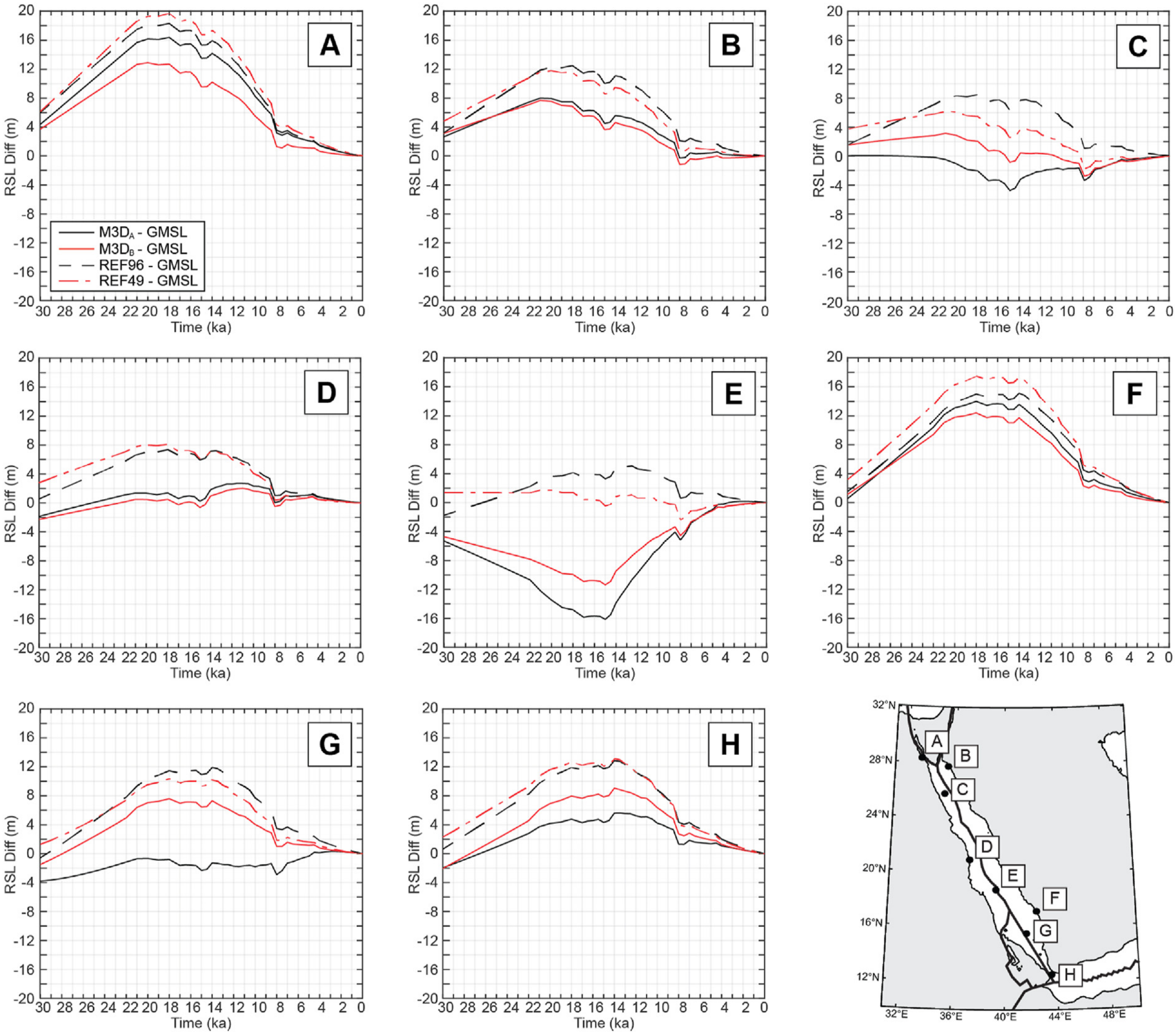

Fig. 5. Difference between RSL and GMSL at each site A-H. The legend is the same for all subfigures.

to present-day values (reflecting a more muted sea-level rise) than the GMSL curves often used in archaeological studies. Paleo-coastlines and the evidence of human settlement that might accompany them are therefore likely submerged at shallower depths than currently predicted. The difference between GMSL and GIA-predicted sea levels also impacts the interpretation and corroboration of paleo-sea levels derived from the location of archaeological sites relative to the modern coastline.

4. Conclusions

We have predicted GIA-induced relative sea-level variations for the Red Sea region from 30 ka to present and have compared results at eight sites with different proximity to the spreading ridge and mouth of the Red Sea. For both 1-D and 3-D GIA simulations, our results indicate that local RSL for the most recent period of deglaciation differs from GMSL in a manner that is both time and location dependent. Furthermore, we find that these discrepancies depend on the choice of GIA modeling – either traditional, purely 1-D viscoelastic Earth structure or 3-D models that include lateral variations in lithospheric thickness and mantle viscosity. Models incorporating 3-D variability tend to result in sea-level predictions that are closer to GMSL than the 1-D simulations, however the discrepancy still reaches a maximum of 6–9 m at the Strait of Bab el-Mandeb at 14 ka, a location previously thought to be a good proxy for GMSL. Discrepancies at other sites within the Red Sea can be even larger. Differences between 1-D and 3-D GIA models typically peak between 10 and 20 m, varying through time and with location within the sea and indicating that the GIA signal obtained by incorporating heterogenous 3-D Earth structure cannot be represented by a simple 1-D radial average. These results illustrate the importance of incorporating GIA into regional sea level studies and applications of such studies more broadly; local sea level in the Red Sea cannot be assumed to correspond to global mean sea level either directly or via a linear scaling.

Funding

This work was supported by the Department of Earth and Planetary Sciences at Harvard University and a Harvard University Center for the Environment undergraduate thesis research support grant to BAP. MJH acknowledges support from the Australian government's Exploring for the Future program. These funding sources were not involved in the conduct of this research or in submitting this research for publication.

Author credit statement

Barra A. Peak: Methodology, Formal analysis, Investigation, Data curation, Writing – original draft, Writing – Edits & Revision, Visualization, Project administration, Funding acquisition. Konstantin Latychev: Methodology, Software, Formal analysis, Data curation, Writing – review & editing. Mark J. Hoggard: Methodology, Software, Writing – review & editing, Funding acquisition. Jerry X. Mitrovica: Conceptualization, Supervision, Project administration, Writing – review & editing.

Declaration of competing interest

The authors declare that they have no known competing financial interests or personal relationships that could have appeared to influence the work reported in this paper.

Acknowledgements

We thank Harriet Lau, Evelyn Powell, Jacky Austermann, Fred Richards, Eelco Rohling, Anthony Purcell, and Céline Grall for helpful feedback and discussion. We thank Bernhard Steinberger and Pippa Whitehouse for careful reviews that improved the manuscript. Map figures were made using the MATLAB package M_Map (Pawlowicz, 2020).

References

Antonioli, F., Furlani, S., Montagna, P., Stocchi, P., 2021. The use of submerged speleothems for sea level studies in the mediterranean sea: a new perspective using glacial isostatic adjustment (GIA). Geosciences 11 (2), 1–37. https://doi.org/10.3390/geosciences11020077.

Austermann, J., Mitrovica, J.X., Latychev, K., Milne, G.A., 2013. Barbados-based estimate of ice volume at Last Glacial Maximum affected by subducted plate. Nat. Geosci. 6 (7), 553–557. https://doi.org/10.1038/ngeo1859.

Austermann, J., Hoggard, M.J., Latychev, K., Richards, F.D., Mitrovica, J.X., 2021. The effect of lateral variations in Earth structure on Last Interglacial sea level. Geophys. J. Int. 227 (July), 1938–1960. https://doi.org/10.1093/gji/ggab289.

Bailey, G.N., 2009. The Red Sea, coastal landscapes, and hominin dispersals. In: Petraglia, M.D., Rose, J.I. (Eds.), The Evolution of Human Populations in Arabia. Springer Verterate Palaeobiology and Palaeoanthropology, Dordrecht, Netherlands, pp. 15–37. https://doi.org/10.1007/978-90-481-2719-1_2.

Bailey, G.N., Sakellariou, D., Alsharekh, A., Al Nomani, S., Devès, M., Georgiou, P., Stavrakakis, S., 2017. Africa-arabia connections and geo-archaeological exploration in the southern red sea: preliminary results and wider significance. In: Under the Sea: Archaeology and Palaeolandscapes of the Continental Shelf, vol. 20. Springer International Publishing, pp. 361–373. https://doi.org/10.1007/978-3-319-53160-1_23.

Bird, P., 2003. An updated digital model of plate boundaries. G-cubed 4 (3). https://doi.org/10.1029/2001GC000252.

Chu, D., Gordon, R.G., 1998. Current plate motions across the Red Sea. Geophys. J. Int. 135 (2), 313–328. https://doi.org/10.1046/j.1365-246X.1998.00658.x.

Conrad, C.P., Lithgow-Bertelloni, C., 2006. Influence of continental roots and asthenosphere on plate-mantle coupling. Geophys. Res. Lett. 33 (5), 2–5. https://doi.org/10.1029/2005GL025621.

Daradich, A., Mitrovica, J.X., Pysklywec, R.N., Willett, S.D., Forte, A.M., 2003. Mantle flow, dynamic topography, and rift-flank uplift of Arabia. Geology 31 (10), 901–904. https://doi.org/10.1130/G19661.1.

Dendy, S., Austermann, J., Creveling, J.R., Mitrovica, J.X., 2017. Sensitivity of Last Interglacial sea-level high stands to ice sheet configuration during Marine Isotope Stage 6. Quat. Sci. Rev. 171, 234–244. https://doi.org/10.1016/j.quascirev.2017.06.013.

Dziewonski, A.M., Anderson, D.L., 1981. Preliminary reference Earth model. Phys. Earth Planet. In. 25 (4), 297–356. https://doi.org/10.1016/0031-9201(81)90046-7.

Eagles, G., Gloaguen, R., Ebinger, C., 2002. Kinematics of the Danakil microplate. Earth Planet Sci. Lett. 203 (2), 607–620. https://doi.org/10.1016/S0012-821X(02)00916-0.

Farrell, W.E., Clark, J.A., 1976. On postglacial sea level. Geophys. J. Roy. Astron. Soc. 46 (3), 647–667. https://doi.org/10.1111/j.1365-246X.1976.tb01252.x.

Fichtner, A., Saygin, E., Taymaz, T., Cupillard, P., Capdeville, Y., Trampert, J., 2013. The deep structure of the north anatolian fault zone. Earth Planet Sci. Lett. 373, 109–117. https://doi.org/10.1016/j.epsl.2013.04.027.

French, S.W., Romanowicz, B., 2015. Broad plumes rooted at the base of the Earth's mantle beneath major hotspots. Nature 525 (7567), 95–99. https://doi.org/10.1038/nature14876.

Goldberg, S.L., Lau, H.C.P., Mitrovica, J.X., Latychev, K., 2016. The timing of the Black Sea flood event: insights from modeling of glacial isostatic adjustment. Earth Planet Sci. Lett. 452, 178–184. https://doi.org/10.1016/j.epsl.2016.06.016.

Goñi, M.F.S., 2020. Regional impacts of climate change and its relevance to human evolution. Evol.Human Sci. 2, 1–27. https://doi.org/10.1017/ehs.2020.56.

Grant, K.M., Rohling, E.J., Bar-Matthews, M., Ayalon, A., Medina-Elizalde, M., Bronk Ramsey, C., Roberts, A.P., 2012. Rapid coupling between ice volume and polar temperature over the past 150,000 years. Nature 491 (7426), 744–747. https://doi.org/10.1038/nature11593.

Hammond, J.O.S., Kendall, J.M., Stuart, G.W., Ebinger, C.J., Bastow, I.D., Keir, D., Wright, T.J., 2013. Mantle upwelling and initiation of rift segmentation beneath the Afar Depression. Geology 41 (6), 635–638. https://doi.org/10.1130/G33925.1.

Hansen, S.E., Gaherty, J.B., Schwartz, S.Y., Rodgers, A.J., Al-Amri, A.M.S., 2008. Seismic velocity structure and depth-dependence of anisotropy in the Red Sea and Arabian shield from surface wave analysis. J. Geophys. Res. 113 (10), 1–16. https://doi.org/10.1029/2007JB005335.

Hay, C.C., Lau, H.C.P., Gomez, N., Austermann, J., Powell, E., Mitrovica, J.X., Wiens, D.A., 2017. Sea level fingerprints in a region of complex earth structure: the case of WAIS. J. Clim. 30 (6), 1881–1892. https://doi.org/10.1175/JCLI-D-16-0388.1.

Hoggard, M.J., Czarnota, K., Richards, F.D., Huston, D.L., Jaques, A.L., Ghelichkhan, S., 2020. Global distribution of sediment-hosted metals controlled by craton edge stability. Nat. Geosci. 13 (7), 504–510. https://doi.org/10.1038/s41561-020-0593-2.

Kendall, R.A., Mitrovica, J.X., Milne, G.A., 2005. On post-glacial sea level – II . Numerical formulation and comparative results on spherically symmetric models. Geophys. J. Int. 161, 679–706. https://doi.org/10.1111/j.1365-246X.2005.02553.x.

Lambeck, K., Purcell, A., Flemming, N.C., Vita-Finzi, C., Alsharekh, A.M., Bailey, G.N., 2011. Sea level and shoreline reconstructions for the Red Sea: isostatic and tectonic considerations and implications for hominin migration out of Africa. Quat. Sci. Rev. 30, 3542–3574. https://doi.org/10.1016/j.quascirev.2011.08.008.

Lambeck, K., Chappell, J., 2001. Sea level change through the last glacial cycle. Science 292 (5517), 679–686. https://doi.org/10.1126/science.1059549.

Lambeck, K., Rouby, H., Purcell, A., Sun, Y., Sambridge, M., 2014. sea level and global ice volumes from the last glacial maximum to the Holocene. Proc. Natl. Acad. Sci. U.S.A. 111 (43), 15296–15303. https://doi.org/10.1073/pnas.1411762111.

Latychev, K., Mitrovica, J.X., Tromp, J., Tamisiea, M.E., Komatitsch, D., Christara, C.C., 2005. Glacial isostatic adjustment on 3-D Earth models: a finite-volume formulation. Geophys. J. Int. 161, 421–444. https://doi.org/10.1111/j.1365-246X.2005.02536.x.

Lisiecki, L.E., Raymo, M.E., 2005. A Pliocene-Pleistocene stack of 57 globally distributed benthic δ18O records. Paleoceanography 20, 1–17. https://doi.org/10.1029/2004PA001071.

Milne, G.A., Mitrovica, J.X., 2008. Searching for eustasy in deglacial sea-level histories. Quat. Sci. Rev. 27 (25–26), 2292–2302. https://doi.org/10.1016/j.quascirev.2008.08.018.

Mitrovica, J.X., Milne, G.A., 2002. On the origin of late Holocene sea-level highstands within equatorial ocean basins. Quat. Sci. Rev. 21, 2179–2190.

Mitrovica, J.X., Milne, G.A., 2003. On post-glacial sea level: I. General theory. Geophys. J. Int. 154, 253–267. https://doi.org/10.1046/j.1365-246X.2003.01942.x.

Mitrovica, J.X., Wahr, J., Matsuyama, I., Paulson, A., 2005. The rotational stability of an ice-age earth. Geophys. J. Int. 161 (2), 491–506. https://doi.org/10.1111/j.1365-246X.2005.02609.x.

Mohriak, W.U., Leroy, S., 2012. Architecture of rifted continental margins and break-up evolution: insights from the south atlantic, north atlantic and Red Sea–Gulf of aden conjugate margins. In: Mohriak, W.U., Danforth, A., Post, P.J., Brown, D.E., Tari, G.C., Nemcok, M., Sinha, S.T. (Eds.), Conjugate Divergent Margins, vol. 369. Geological Society, London, Special Publications, London, pp. 497–535. https://doi.org/10.1144/SP369.17.

Pawlowicz, R., 2020. M_Map: A Mapping Package for MATLAB. Retrieved from. https://www.eoas.ubc.ca/∼rich/map.html.

Peltier, W.R., 2004. Global glacial isostasy and the surface of the ice-age earth: the ICE-5G (VM2) model and GRACE. Annu. Rev. Earth Planet Sci. 32, 111–149. https://doi.org/10.1146/annurev.earth.32.082503.144359.

Peltier, W.R., Fairbanks, R.G., 2006. Global glacial ice volume and Last Glacial Maximum duration from an extended Barbados sea level record. Quat. Sci. Rev. 25 (23–24), 3322–3337. https://doi.org/10.1016/j.quascirev.2006.04.010.

Peresani, M., Monegato, G., Ravazzi, C., Bertola, S., Margaritora, D., Breda, M., Zerboni, A., 2021. Hunter-gatherers across the great adriatic-Po region during the last glacial maximum: environmental and cultural dynamics. Quat. Int. 581 (582). https://doi.org/10.1016/j.quaint.2020.10.007.

Pico, T., Mitrovica, J.X., Ferrier, K.L., Braun, J., 2016. Global ice volume during MIS 3 inferred from a sea-level analysis of sedimentary core records in the Yellow River Delta. Quat. Sci. Rev. 152, 72–79. https://doi.org/10.1016/j.quascirev.2016.09.012.

Powell, E.M., Pan, L., Hoggard, M.J., Latychev, K., Gomez, N., Austermann, J., Mitrovica, J.X., 2021. The impact of 3-D Earth structure on far-field sea level following interglacial West Antarctic Ice Sheet collapse. Quat. Sci. Rev. 273, 107256. https://doi.org/10.1016/j.quascirev.2021.107256.

Purser, B.H., Bosence, D.W.J. (Eds.), 1998. Sedimentation and Tectonics in Rift Basins: Red Sea - Gulf of Aden, first ed. Springer, Dordrecht, Netherlands. https://doi.org/10.1007/978-94-011-4930-3.

Richards, F., Hoggard, M., White, N., Ghelichkhan, S., 2020. Quantifying the relationship between short-wavelength dynamic topography and thermomechanical structure of the upper mantle using calibrated parameterization of anelasticity. J. Geophys. Res. Solid Earth 125 (9). https://doi.org/10.1029/2019JB019062.

Ritsema, J., Deuss, A., Van Heijst, H.J., Woodhouse, J.H., 2011. S40RTS: a degree-40 shear-velocity model for the mantle from new Rayleigh wave dispersion, teleseismic traveltime and normal-mode splitting function measurements. Geophys. J. Int. 184, 1223–1236. https://doi.org/10.1111/j.1365-246X.2010.04884.x.

Ritsema, Jeroen, Van Heijst, H.J., Woodhouse, J.H., 1999. Complex shear wave velocity structure imaged beneath Africa and Iceland. Science 286 (5446), 1925–1931. https://doi.org/10.1126/science.286.5446.1925.

Rohling, E.J., Fenton, M., Jorissen, F.J., Bertrand, P., Ganssen, G., Caulet, J.P., 1998. Magnitudes of sea-level lowstands of the past 500,000 years. Nature 394, 162–165. https://doi.org/10.1038/28134.

Rohling, E.J., Grant, K.M., Hemleben, C., Siddall, M., Hoogakker, B.A.A., Bolshaw, M., Kucera, M., 2008. High rates of sea-level rise during the last interglacial period. Nat. Geosci. 1, 38–42. https://doi.org/10.1038/ngeo.2007.28.

Schaeffer, A.J., Lebedev, S., 2013. Global shear speed structure of the upper mantle and transition zone. Geophys. J. Int. 194 (1), 417–449. https://doi.org/10.1093/gji/ggt095.

Shakun, J.D., Raymo, M.E., Lea, D.W., 2016. An early Pleistocene Mg/Ca-δ18O record from the Gulf of Mexico: evaluating ice sheet size and pacing in the 41-kyr world. Paleoceanography 31 (7), 1011–1027. https://doi.org/10.1002/2016PA002956.

Siddall, M., Smeed, D.A., Hemleben, C., Rohling, E.J., Schmelzer, I., Peltier, W.R., 2004. Understanding the Red Sea response to sea level. Earth Planet Sci. Lett. 225, 421–434. https://doi.org/10.1016/j.epsl.2004.06.008.

Siddall, M., Rohling, E.J., Almogi-Labin, A., Hemleben, C., Meischner, D., Schmelzer, I., Smeed, D.A., 2003. Sea-level fluctuations during the last glacial cycle. Nature 423, 853–858. https://doi.org/10.1038/nature01687.1.

Werner, F., Lange, K., 1975. A bathymetric survey of the sill area between the Red Sea and the Gulf of Aden. Geologisches Jahrbuch, Mineralogie, Petrographie, Geochemie, Lagerstattenkunde, D (13), 125–130.

White, T.D., Asfaw, B., Degusta, D., Gilbert, H., Richards, G.D., Suwa, G., Howell, F.C., 2003. Pleistocene Homo sapiens from middle awash, Ethiopia. Nature 423, 742–747. https://doi.org/10.1038/nature01669.

Wilson, J.W.P., Roberts, G.G., Hoggard, M.J., White, N.J., 2014. Cenozoic epeirogeny of the Arabian Peninsula from drainage modeling. G-cubed 15 (10), 3723–3761. https://doi.org/10.1002/2014GC005283.